

Electron-Spin and Electron-Orbital Dependence of the Tunnel Coupling in Laterally Coupled Double Vertical Dots

T. Hatano,^{1,*} M. Stopa,¹ T. Yamaguchi,¹ T. Ota,¹ K. Yamada,¹ and S. Tarucha^{1,2}

¹*Tarucha Mesoscopic Correlation Project, ERATO, JST, Atsugi-shi, Kanagawa 243-0198, Japan*

²*Department of Applied Physics, University of Tokyo, Hongo, Bunkyo-ku, Tokyo 113-0033, Japan*

(Received 29 December 2003; published 6 August 2004)

We employ a new laterally coupled, vertical double dot with a tunable tunnel-coupling gate in a parallel configuration to study the electron spin and orbital dependence of quantum mechanical tunnel coupling on the size of the honeycomb vertices in the small electron numbers regime. We find a transition from the weak coupling regime, where fluctuations in tunnel coupling due to varying electron configuration dominate the anticrossings, to a regime where the two dots coalesce. We apply a magnetic field to ascertain the orbital angular momenta of the Fermi surface eigenstates, which correlate with anticrossing size, and we identify spin pairs with congruent behavior.

DOI: 10.1103/PhysRevLett.93.066806

PACS numbers: 73.63.Kv, 73.23.Hk

Double quantum dots, or artificial molecules, are emerging as important systems for quantum computing and spintronics applications as well as providing laboratories for studying the physics of molecular bonding, which forms the basis of all chemical and biochemical processes. Essential to the structure of these two-center systems is the competition between Coulomb interaction among the electrons and quantum mechanical electron tunneling between the two constituent “atoms.” While proposed quantum computing schemes [1,2] require tunable tunnel coupling to mediate the exchange interaction between electrons centered at the two sites on the one hand, the freedom to control interactions and electron numbers in artificial molecules permit investigation of chemical bonding on the other hand [3,4].

Heretofore, double dot studies have been carried out in either lateral semiconductor devices [5], where controllable access to the small electron numbers regime has been evasive, or in vertical, triple barrier structures [6,7], where the interdot coupling can be tuned only marginally with a parallel magnetic field [8]. While recent progress in reducing electron numbers in lateral structures has occurred first in single [9] and then in double dot systems [10], and the electron number has indeed been reduced down to zero electrons per dot [11], there has as yet been no detailed study of the eigenfunction dependent interdot tunnel-coupling strength and its influence on electronic structure as displayed, for example, in the characteristic “honeycomb” stability diagram of the double dot.

In this Letter we present results of a study of transport through a unique hybrid vertical-lateral quantum double dot (Fig. 1), which combines small electron numbers (we estimate that N_1, N_2 are both less than or equal to 12) and adjustable interdot coupling. We measure the honeycomb stability diagram, and, in particular, the length of honeycomb vertices (“anticrossings”), and show evidence that

quantum mechanical level repulsion of pairs of states at the Fermi surface makes a significant contribution to these anticrossings. Evolution of the honeycomb with barrier height shows a rapid decrease in the dispersion of anticrossings, which we attribute to a merging of the dots. We apply a magnetic field perpendicular to the dot planes to determine the angular momenta of selected eigenstates at the dot Fermi surfaces and we display a correlation between these angular momenta and the anticrossing size, further demonstrating the significance of the tunnel coupling. Finally, the magnetic field dependence allows us to identify certain spin pairs of eigenstates whose orbitals are identical and whose anticrossing behavior is strongly correlated.

Our device shown schematically in Fig. 1(a) is made from a double-barrier heterostructure (DBH) [12]. The DBH consists of an undoped 12 nm InGaAs well and undoped AlGaAs barriers of thicknesses 8.5 and 7.0 nm

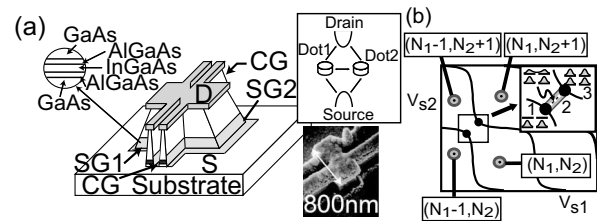


FIG. 1. (a) Structure of double quantum dot device. Top and bottom contacts serve as drain and source electrodes. Side gates (SG1, SG2) tune electron number in each dot; two center gates (CG) tune tunnel coupling between dots. Center insets: Schematic figure of electric transport and scanning electron micrograph of device. (b) Schematic honeycomb stability diagram in the V_{s1} - V_{s2} plane, stable electron numbers in dots 1 and 2 noted. Inset: Close-up of single anticrossing, showing evolution of states along central diagonal. Delocalization region connects two “triple points” (black dots). Energies and descriptions of states 1, 2, and 3 in text.

(the thinner one is closest to the substrate). Current flows vertically through two dots which are coupled laterally (center inset of Fig. 1). There are four split gates, two of which (side gates) tune the number of electrons in each dot independently, and the remaining two (center gates), which are usually swept in tandem, tune the interdot tunnel barrier height.

The scanning electron micrograph of our device is shown in the center inset of Fig. 1(a). The double quantum dot is located inside the $0.35 \times 0.8 \mu\text{m}^2$ mesa. Four $0.15 \mu\text{m}$ wide line mesas emerge from the sides of the double dot mesa. The mesas are sufficiently thin that current flows only through the top metal contact. The line mesas split the surrounding Schottky gate metal [13]. Measurements are carried out in a dilution refrigerator at temperature 60 mK. The source-drain voltage is fixed at $V_{sd} = 8 \mu\text{V}$.

Sweeping the side gate voltages V_{s1} , V_{s2} at several values of the center gate voltage V_c reveals a series of Coulomb oscillations (Fig. 2) which display a double dot honeycomb pattern but with substantial curvature of the oscillations particularly near the anticrossings. For the weakest coupling, most negative V_c case [Fig. 2(a)], the gap size fluctuates substantially from one anticrossing to another. The charging energies of the two dots, as determined by nonlinear transport measurements, are about 1 meV. Using this to establish the gate-dot capacitances, we find that the anticrossing energies in Fig. 2(a) range from 0.4 meV down to 0.1 meV. For increased V_c (smaller barrier) the anticrossing gaps widen until, at $V_c = -2.0$ V [Fig. 2(b)], many of the anticrossings are barely discernible. In this limiting case the dots have merged (the Fermi surface of the dots is above the interdot saddle point) and the charging energy has dropped to 0.4 meV, about half that of the single dots in Fig. 2(a). Note that this behavior is not homogeneous throughout the plane in Fig. 2(b) but rather depends on side gate voltages. This cross capacitive effect results in an increase of barrier height as the side gates become less negative, suggesting that the laterally placed gates tend to pull the dots apart even as they induce more electrons.

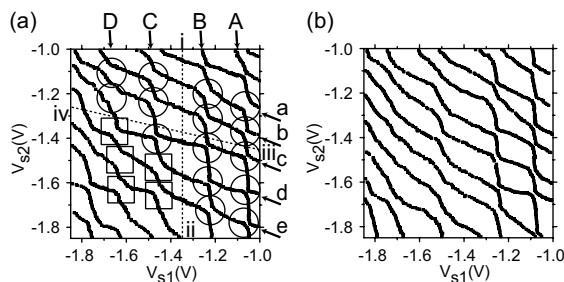


FIG. 2. (a) Coulomb peak positions in V_{s1} - V_{s2} plane for center gate voltage $V_c = -2.4$ V and (b) $V_c = -2.0$ V. Anticrossings in squares and circles in (a) are used for statistical analysis (see Fig. 3). Those in squares show different dependence on angular momenta of states (see Fig. 4).

The “classical” theory of double dots [14] ascribes these anticrossings to interdot capacitance. For smaller dots this capacitive energy reduces to an interdot Coulomb matrix element, V_{inter} , between the two localized states at the Fermi surface of each dot [15]. More generally, the structure of the anticrossing is illustrated in Fig. 1(b) and its inset. Along a diagonal vertex the ground state evolves from (1) a filled core (here indicated by two filled states) with an empty level in each dot to (2) the anticrossing regime where a single added electron is delocalized between two, generally nonequivalent, orbitals in the two dots to (3) a final state where two added electrons occupy states localized about the individual dots [16]. The localizing effect of adding the second electron, which produces a state similar to the Heitler-London (HL) state [3] for the two electrons at the Fermi surface, occurs when $V_{\text{intra}} - V_{\text{inter}} \geq t$, where V_{intra} is a typical intradot Coulomb matrix element and t is the tunnel (i.e., symmetric-antisymmetric) splitting. Ignoring interdot exchange Coulomb matrix elements [17] and treating both V_{intra} and V_{inter} as independent of eigenstate, the energies of the three states are $E_1 = 2\varepsilon_1 + V_{\text{inter}} + 2e\phi$, $E_2 = 2\varepsilon_1 + E_S + 2V_{\text{inter}} + V_{\text{intra}} + 3e\phi$, and $E_3 = 2\varepsilon_1 + 2\varepsilon_2 + 4V_{\text{inter}} + 2V_{\text{intra}} + 4e\phi$, where ϕ is the electrostatic potential of the bottom of the two dots (assumed equal) which depends in a complex way on the voltages and the capacitance matrix. Also, $\varepsilon_{1,2}$ are the bare energies of the two levels and E_S is the energy of the delocalized symmetric state formed from the hybridization of state 2 between dots 1 and 2, i.e., $E_S = \varepsilon_2 - t$. If ϕ and ϕ' are the externally applied potential at the two triple points where $E_1 = E_2$ and $E_2 = E_3$, respectively [Fig. 1(b) inset], it is then apparent that $\Delta V \equiv e(\phi - \phi') = 2\varepsilon_2 - 2E_S + V_{\text{inter}} = 2t + V_{\text{inter}}$.

The anticrossing data are summarized in Fig. 3 where the average gap energies $\overline{\Delta V}$ and their standard deviations σ are shown for three center gate voltages. Averages are taken over the anticrossings which are highlighted with boxes or circles in Fig. 2(a). In the HL regime, where each electron is localized by Coulomb correlation about one dot, the interdot Coulomb matrix element is known to be largely insensitive to barrier height [2] and forms the

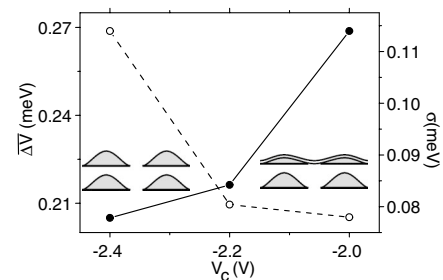


FIG. 3. Center gate voltage V_c dependencies of mean value $\overline{\Delta V}$ (solid line) and standard deviation σ (dashed line) of tunnel-coupling energy ΔV , calculated using anticrossings enclosed by circles and squares in Fig. 2(a).

lower bound for the anticrossing gap energy. The tunneling strength t is, however, exponentially sensitive to barrier penetration. Dispersion of anticrossings where t is a significant component will, therefore, be greater. For $V_c = -2.4$ V, if we take for the mean of the tunnel splitting $2\bar{t} = \overline{\Delta V} - V_{\text{inter}}$ and use for V_{inter} the smallest value of $\Delta V \approx 0.08$ meV, then $2\bar{t} \approx 0.125$ meV, which implies $\sigma/2\bar{t} \approx 0.92$ [18]. We attribute the somewhat surprising fact that $2\bar{t} > V_{\text{inter}}$ to the fact that the dots are bounded by the three dimensional electron gases of the leads and hence screening is strong.

As V_c increases, $\overline{\Delta V}$ also increases and σ decreases. This suggests that the dots coalesce at the Fermi surface, whereupon t increases to become the level separation in the coalesced dot and, simultaneously, the distinction between V_{intra} and V_{inter} vanishes, so that $t > V_{\text{intra}} - V_{\text{inter}}$. In this regime, it is energetically favorable to occupy both spin states of the symmetric wave function (cf. inset of level schematic in Fig. 3) rather than form the localized HL states. Repeating the analysis of the gap size, we find that now $E_3 = 2\varepsilon_1 + 2E_S + (7V_{\text{inter}}/2) + (5V_{\text{intra}}/2) + 4e\phi$ and consequently $e(\phi - \phi') = (1/2) \times (V_{\text{inter}} + V_{\text{intra}})$; i.e., the gaps are independent of the strongly fluctuating t , and σ decreases.

Each Coulomb peak, away from the anticrossing areas, corresponds to addition of an extra electron to a localized state in one of the two dots. The set of peaks along the V_{s1} (V_{s2}) axis are labeled by A, B, C, D (a, b, c, d, e) in Fig. 2(a). The coupling of the associated states at the Fermi surface to a magnetic field B is paramagnetic for low B . Hence the dependence of these Coulomb peak positions on B , measured along dotted lines $i-ii$ and $iii-iv$ in Fig. 2(a) and plotted in Figs. 4(a) and 4(b), reveal the angular momenta of the Fermi surface states.

It appears from the B dependence that peak pairs A and B , C and D , a and b , and d and e are spin-pair orbitals. The insets of Figs. 4(a) and 4(b) exhibit the correlation functions [19] for anticrossing size computed from the data in Fig. 2(a). The pairs A and B , C and D for dot 1 have strongly correlated anticrossings, confirming their identity as spin pairs. Dot 2, however, is more ambiguous. While d and e are strongly correlated, a and b are *anti-correlated*. Further, orbital c shows a strong correlation with b . For *single* vertical quantum dots with $N \geq 6$, sequential Coulomb oscillations can often be identified with spin-paired orbitals until a first orbital crossing occurs, typically around $B \sim 0.1$ T [12]. If, however, orbital degeneracy occurs at $B = 0$ (due to symmetry or accidental degeneracy) then Hund's rule can result in the sequential filling of parallel spins in different orbitals. In this case, a very small magnetic field breaks the degeneracy and changes the level filling sequence. Thus we speculate that a and b are a spin pair at $B \neq 0$, but for $B = 0$ the two Coulomb oscillations that represent spin-pair orbitals are those labeled b and c .

Naively we expect an increase in barrier penetration, and hence anticrossing gap, with angular momentum due to the centrifugal barrier. We have calculated tunnel matrix elements $t_{nm, NM}$ [20], where n, N are the principal quantum numbers and m, M are the angular momentum quantum numbers, employing Fock-Darwin [21] states on two adjacent circularly parabolic wells (at $B = 0$). Plotted versus the product $|m||M|$ in Fig. 4(c), a rising trend is clear; however, the $t_{nm, NM}$ also depend clearly on n and N . By contrast, the experimental data on the anticrossing gaps, Fig. 4(d), show two simple linear trends with $|m_i||M_j|$. Thus the data cannot be explained entirely with the angular momentum dependence of the coupling

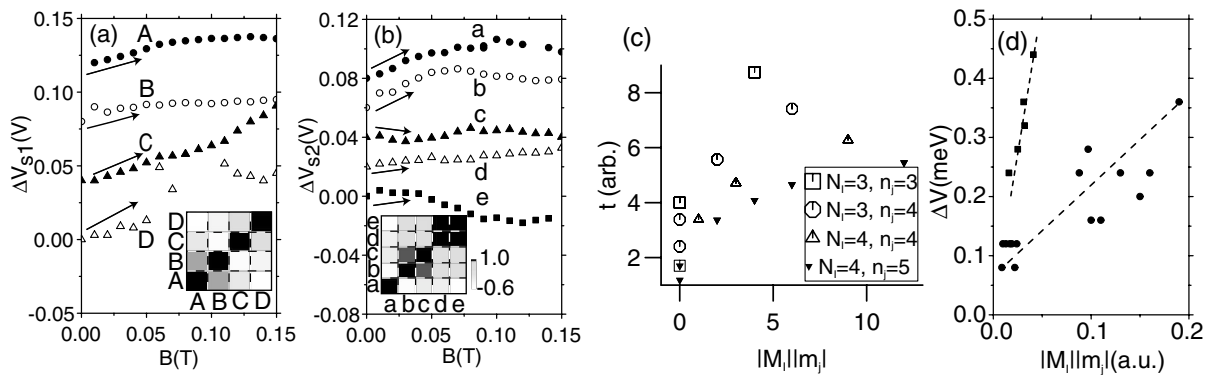


FIG. 4. (a) Magnetic field dependencies of Coulomb peak position shifts, ΔV_{s1} , measured along the dashed line $i-ii$ of Fig. 2(a). Inset: Correlation function [19] of the anticrossing widths for states in dot 1. (b) Same for Coulomb peaks position shifts ΔV_{s2} along dashed line $iii-iv$ of Fig. 2(a). The labeled Coulomb oscillations correspond to those of Fig. 2(a). Inset: Same as inset in (a) for dot 2. In 2(a) and 2(b) main panels, ΔV_{s1} (ΔV_{s2}) indicates the shift value from V_{s1} (V_{s2}) at $B = 0$ T. Here ΔV_{s1} and ΔV_{s2} are smoothed across five magnetic field points and the plots are shifted by multiples of 0.02 V. (c) Tunnel coefficient calculated from Fock-Darwin spectra for two adjacent parabolic wells versus product of state angular momenta $|M_i||m_j|$. N_i, n_j are principle quantum numbers. (d) Anticrossing gap sizes, relative to mean $\overline{\Delta V}$, versus product of angular momenta of Fermi surface states derived from slopes at $B = 0$ in (a) and (b). Solid squares indicate gaps inside squares and solid circles for gaps inside circles in Fig. 2(a).

constants, except within very limited regions of quantum numbers. In addition to the quantum mechanical coupling, the Coulomb component of the anticrossing may itself also be expected to depend on $|m|$ and $|M|$ through their influence on wave function overlap and hence on direct and exchange matrix elements.

The points along the steeper slope [squares in Fig. 4(d)], corresponding to the anticrossings in boxes in Fig. 2(a), occur for larger (negative) side gate voltages where, even for $V_c = -2.4$ V, the dots may have merged. In this case, the two electrons at the Fermi surface both occupy the symmetric, delocalized orbital (spin up and spin down) and the direct Coulomb matrix element will increase with the wave function probability in the saddle point. While this probability will also depend on angular momenta of the participating original states, it is unclear whether the angular momenta of the independent dot states are still meaningful in this coalesced regime. In summary, the anticrossings show clear increase with angular momenta, but elucidating the trend and its relationship to the Coulomb and quantum mechanical electronic structure requires further data and theoretical calculations.

In conclusion, we have employed a unique vertical/lateral hybrid double dot to explore the effects of quantum mechanical tunneling and many body correlations on the anticrossings of the honeycomb stability diagram. The structure of the honeycomb stability diagram statistically separates into two regimes depending on whether Coulomb correlation, determined by $V_{\text{intra}} - V_{\text{inter}}$, is greater or less than quantum mechanical tunnel coupling t . We have also shown that spin-paired states show correlated anticrossings and that the gap sizes exhibit a clear increasing trend with participating angular momenta.

We thank T. Sato, S. Teraoka, T. Inoshita, W. Izumida, A. Shibatomi, T. Maruyama, K. Ono, S. Amaha, Y. Nishi, S. Sasaki, and D.G. Austing for experimental help and useful discussions. Part of this work is financially supported by the Grant-in-Aid for Scientific Research A (No. 40302799) and by SORST-JST. This work is supported by the DARPA-QUIST program (DAAD19-01-1-0659).

*Electronic address: hatano@tarucha.jst.go.jp

- [1] D. Loss and D.P. DiVincenzo, Phys. Rev. A **57**, 120 (1998).
 [2] J. Schliemann, D. Loss, and A.H. MacDonald, Phys. Rev. B **63**, 085311 (2001).

- [3] *Electron Correlations in Molecules and Solids*, edited by P. Fulde (Springer-Verlag, Berlin, 1995).
 [4] M. Rontani, F. Troiani, U. Hohenester, and E. Molinari, Solid State Commun. **119**, 309 (2001).
 [5] C. Livermore *et al.*, Science **274**, 1332 (1996); J.M. Golden and B.I. Halperin, Phys. Rev. B **53**, 3893 (1996); K.A. Matveev, L.I. Glazman, and H.U. Baranger, Phys. Rev. B **54**, 5637 (1996).
 [6] D.G. Austing *et al.*, Physica (Amsterdam) **249-251B**, 206 (1998).
 [7] K. Ono *et al.*, Science **297**, 1313 (2002).
 [8] Y. Tokura *et al.*, Physica (Amsterdam) **6E**, 676 (2000).
 [9] M. Ciorga *et al.*, Phys. Rev. B **61**, R16 315 (2000).
 [10] A.W. Holleitner *et al.*, Science **297**, 70 (2002); A.W. Holleitner *et al.*, Phys. Rev. Lett. **87**, 256802 (2001).
 [11] J.M. Elzerman *et al.*, Phys. Rev. B **67**, 161308 (2003); M. Pioro-Ladrière *et al.*, Phys. Rev. Lett. **91**, 026803 (2003); I.H. Chan *et al.*, cond-mat/0309205.
 [12] S. Tarucha *et al.*, Phys. Rev. Lett. **77**, 3613 (1996).
 [13] D.G. Austing, T. Honda, and S. Tarucha, Semicond. Sci. Technol. **12**, 631 (1997).
 [14] W.G. van der Wiel *et al.*, Rev. Mod. Phys. **75**, 1 (2003).
 [15] We employ the notation and conventions introduced in Y. Tokura, D.G. Austing, and S. Tarucha, J. Phys. Condens. Matter **11**, 6023 (1999).
 [16] Note that degeneracy in the level structure of either dot complicates this analysis. Indeed, the magnetic field data in Fig. 4 seem to indicate one instance of degeneracy at $B = 0$. However, asymmetry in the bare frequencies along perpendicular directions need be only of order 2% in order that the splitting of levels in a shell are comparable to the tunnel splitting. Thus, nondegenerate levels are a reasonable assumption.
 [17] The exchange contribution need not be negligible when the coupling is strong (see Ref. [2] for details); however, here we can simply assume that our V_{inter} is the exchange-modified interaction between the dots.
 [18] We note that if the distribution of t were given simply by the Porter-Thomas distribution [cf. T.A. Brody *et al.*, Rev. Mod. Phys. **53**, 385 (1981)], this ratio would instead be $\sqrt{2}$. However, we are presumably far from the ergodic regime.
 [19] Specifically, the correlation is defined as

$$C_{i,j} = \frac{\sum_J (\Delta V_{i,J} - \overline{\Delta V}_i)(\Delta V_{j,J} - \overline{\Delta V}_j)}{\sqrt{\sum_J (\Delta V_{i,J} - \overline{\Delta V}_i)^2} \sqrt{\sum_J (\Delta V_{j,J} - \overline{\Delta V}_j)^2}},$$

where $\Delta V_{i,J}$ is the anticrossing value of the orbital i and J , and $\overline{\Delta V}_i$ is the average anticrossing size for orbital i (averaged over J).

- [20] J. Bardeen, Phys. Rev. Lett. **6**, 57 (1961).
 [21] V. Fock, Z. Phys. **47**, 446 (1928); C.G. Darwin, Proc. Cambridge Philos. Soc. **27**, 86 (1930).